Since all the crystal structures of thiamin, its derivatives, and their metal complexes are mostly in the *F* configuration, with only a few exceptions in the *S* configuration, including its active aldehyde derivatives, the role of the N(4'α)-$H_2$ group to act directly as a proton donor or acceptor is questionable. As pointed out by Sax et al.,[12a] the deprotonation of the O(11)-H proton makes the S(1)···O(11) interaction even stronger and stabilizes the preferred *S* conformation. Thus, the S(1) atom is better suited sterically and electronically to facilitate this deprotonation than the frequently mentioned N(4'α) amino group.[12b] Since $Hg^{2+}$ coordination and (more generally), metal coordination *follows* the formation of the active aldehyde derivative of thiamin, thereby *not* influencing the original *S* conformation,[28] it seems reasonable to accept this hypothesis. To provide further confirmation, however, the elucidation of many similar structures will have to be done.

(28) All the complexes of the IIB group metals, as well as the first row transition metals ($Co^{2+}$, $Ni^{2+}$, etc.), with these ligands are isostructural in the solid state, having identical (band by band) IR and Raman spectra.

**Acknowledgment.** This work was supported in part by the Greek Ministry of Research and Technology.

**Registry No.** Zn(HBT)$Cl_3$, 128842-99-9; Cd(HBT)$Cl_3$, 128869-02-3; Hg(HBT)$Cl_3$·$H_2O$, 128843-00-5; Zn(HCMT)$Cl_3$, 128843-01-6; Cd(HCMT)$Cl_3$, 128843-02-7; Hg(HCMT)$Cl_3$, 128843-03-8; Zn(HBT)$Br_3$, 128843-04-9; Cd(HBT)$Br_3$, 128843-05-0; Hg(HBT)$Br_3$, 128843-06-1; Zn(HCMT)$Br_3$, 128843-07-2; Cd(HCMT)$Br_3$, 128843-08-3; Hg(HCMT)$Br_3$, 128843-09-4; $D_2$, 7782-39-0.

**Supplementary Material Available:** Tables of final temperature factors (Table A), final atomic coordinates (Table B), best-weighted least-squares planes for the pyrimidine, thiazole, and benzyl rings (Table C), and intramolecular separations between pairs of atoms (Table D), and figure of the unit cell packing diagram for the complex Hg(HBT)$Cl_3$·$H_2O$ (4 pages). Ordering information is given on any current masthead page.

# The Tetranuclear Trianion $[Fe_4Te_4(SC_6H_5)_4]^{3-}$: Crystal and Molecular Structure and Magnetic Properties

**Pierluigi Barbaro,[†] Alessandro Bencini,[†] Ivano Bertini,*[,†] Fabrizio Briganti,[†] and Stefano Midollini[‡]**

*Contribution from the Dipartimento di Chimica, Università di Firenze, and I.S.S.E.C.C., C.N.R., Firenze, Italy.* *Received November 6, 1989*

**Abstract:** The synthesis and the spectroscopic, magnetic, and structural characterization of the compound $(Et_4N)_3[Fe_4Te_4(SPh)_4]$ (Ph = $C_6H_5$) are reported. The complex crystallizes in the orthorombic system, space group *Fdd*2, with $a$ = 39.976 (5) Å, $b$ = 24.963 (6) Å, and $c$ = 12.200 (2) Å. The molecular structure consists of discrete tetranuclear anions $[Fe_4Te_4(SPh)_4]^{3-}$ with a cubane-like $[Fe_4Te_4]^+$ unit. The magnetic behavior has been interpreted by using the Heisenberg-Dirac-Van Vleck exchange coupling model with antiferromagnetic interactions between the iron centers. The ground state has been found to correspond to a total spin state $S$ = 3/2. EPR and $^1$H-NMR spectra are also reported. The available magnetic data of $Fe_4S_4$ and $Fe_4Se_4$ clusters have also been interpreted providing the correct ground state. The increased distance between the irons in the $[Fe_4Te_4]^+$ core in comparison to the analogous $[Fe_4S_4]^+$ and $[Fe_4Se_4]^+$ cores decreases the antiferromagnetic coupling among the iron ions. The influence of geometric parameters on the exchange pathways between iron atoms in this class of compounds is discussed within the orbital model of the exchange interaction using EHMO theory.

## Introduction

The synthesis of low molecular weight analogues of four iron ferredoxins and the study of their spectroscopic, magnetic, and structural properties have been the subject of extensive investigations.[1] From all these studies the isoelectronic nature of the synthetic clusters with Fe-S proteins which occur in important biological redox processes has appeared.[2-4]

Despite the number of experimental and theoretical efforts, the electronic structure of these systems is still not completely determined, and an active area of research is devoted to the synthesis of new clusters which could be investigated with the largest possible numbers of experimental techniques in order to get a deeper insight into their electronic structure. In the case of $Fe_2S_2$ proteins and in their synthetic analogues the low-lying energy levels have been successfully interpreted within the Heisenberg-Dirac-Van Vleck exchange coupling theory, which reduces the electronic coupling between the individual iron centers to a formal magnetic coupling between localized spins.[5] In a number of $Fe_3S_4$ clusters and proteins Mössbauer and magnetically perturbed Mössbauer studies have shown that some electron delocalization should occur.[6] In particular the magnetic structure unit $Fe_3S_4^+$, formally containing one Fe(III) and two Fe(II) centers, has been interpreted assuming complete valence delocalization between two iron centers and exchange interaction of this delocalized couple with the other iron center.[6] A similar picture has been adopted to describe the nature of the low-lying energy levels in some $Fe_4S_4$ clusters.[7]

With the aim to provide new information for the understanding of the properties of the $Fe_4X_4$ clusters we wish to report here the synthesis, crystal and molecular structure, and magnetic and spectroscopic properties of $(Et_4N)_3[Fe_4Te_4(SPh)_4]$, a molecule

* Address correspondence to Prof. Ivano Bertini at the Department of Chemistry, University of Florence, Via G. Capponi 7, 50121 Firenze, Italy.
[†] Università di Firenze.
[‡] I.S.S.E.C.C., C.N.R.

(1) Berg, J. M.; Holm, R. H. In *Iron Sulphur Proteins; Metal Ions in Biology Series*; Spiro T. G., Ed.; John Wiley & Sons: New York, 1982; Vol. 4, Chapter 1.
(2) (a) Carney, M. J.; Papaefthymiou, G. C.; Whitener, M. A.; Spartalian, K.; Frankel, R. B.; Holm, R. H. *Inorg. Chem.* **1988**, *27*, 346-352. (b) Hagen, K. S.; Reynolds, J. G.; Holm, R. H. *J. Am. Chem. Soc.* **1981**, *103*, 4054.
(3) Hill, C. L.; Renaud, J.; Holm, R. H.; Mortenson, L. E. *J. Am. Chem. Soc.* **1977**, *99*, 2549-2557.
(4) Carney, M. J.; Papaefthymiou, G. C.; Spartalian, K.; Frankel, R. B.; Holm, R. H. *J. Am. Chem. Soc.* **1988**, *110*, 6084-6095.
(5) Papaefthymiou, V.; Girerd, J.-J.; Moura, I.; Moura, J. J. G.; Munck, E. *J. Am. Chem. Soc.* **1987**, *109*, 4703-4710.
(6) Münck, E.; Papaefthymiou, V.; Surerus, K. K.; Girerd, J. J. *Metal Clusters in Proteins*; Que, L., Jr., Ed.; ACS Symposium Series 372; American Chemical Society: Washington, DC, 1988; p 302.
(7) Noodleman, L. *Inorg. Chem.* **1988**, *27*, 3677-79.

0002-7863/90/1512-7238$02.50/0 

Table I. Crystallographic Data for $(Et_4N)_3[Fe_4Te_4(SPh)_4]$

| | |
|---|---|
| $C_{48}H_{80}Fe_4N_3S_4Te_4$ | mol wt = 1561.21 |
| $a$ = 39.976 (5) Å | space group *Fdd*2 |
| $b$ = 24.963 (6) Å | $T$ = 21 °C |
| $c$ = 12.200 (2) Å | $\lambda$ = 0.71069 (Mo K$\alpha$) Å |
| $\alpha$ = 90.00 (deg) | $\rho_{calcd}$ = 1.7035 g cm$^{-3}$ |
| $\beta$ = 90.00 (deg) | $\mu$ = 29.8 cm$^{-1}$ |
| $\gamma$ = 90.00 (deg) | $R$ = 4.52% |
| $V$ = 12174.63 Å$^3$ | $R_W$ = 4.47% |
| $Z$ = 8 | |

containing the cubane-like cluster $[Fe_4Te_4(SPh)_4]^{3-}$ formally formed by one Fe(III) and three Fe(II) centers. The X-ray structure parameters, the magnetic properties, and the $^1$H-NMR spectra are compared with those of the analogous $Fe_4S_4$ and $Fe_4Se_4$ derivatives.

A model is developed to account for the magnetic properties of all the clusters containing three iron(II) and one iron(III) ions. Finally, the observed decrease in the magnetic coupling on passing from the S to the Te derivative has been related to variations of geometrical parameters on the basis of extended Hückel calculations.

## Experimental Section

**Preparation of Compounds.** All manipulations were performed under strictly anaerobic conditions in dinitrogen atmosphere owing to the sensitivity of all the components to dioxygen. Solvents were degassed immediately prior to use. Acetonitrile and diethyl ether were distilled from $CaH_2$ and $LiAlH_4$, respectively. The commercially available solution of $LiEt_3BH$ 1 M in THF, super-hydride (Aldrich), was used. Elemental tellurium was used in its powdered form and stored in a desiccator. The synthesis of $(Et_4N)_2Fe(SPh)_4$ was described elsewhere.[2b] All the other reagents and solvents were commercial products and were used without further purification.

**$(Et_4N)_3[Fe_4Te_4(SPh)_4]$.** Twelve milliliters (12.0 mmol) of $LiEt_3BH$ in THF solution was added under magnetic stirring and in the dark to 762 mg (6.0 mmol) of elemental tellurium causing a slow gas evolution. The suspension gradually turned to a milky violet color. It was allowed to stir for 20 min since no residue of tellurium was observed. The previous suspension, diluted with 20 mL of $CH_3CN$, was added dropwise under vigorous stirring to a suspension of 4.5 g (6.0 mmol) of $(Et_4N)_2Fe(SPh)_4$ in 20 mL of $CH_3CN$ resulting in the immediate formation of a deep yellow-brown solution which was decanted and then allowed to stand at −25 °C overnight. Black needle-shaped crystals separated out. They were filtered, washed with ether, and dried under nitrogen [yield 390 mg (17%). Anal. Calcd for $C_{48}H_{80}Fe_4N_3S_4Te_4$: C, 36.93; H, 5.17; Fe, 14.31; N, 2.69. Found: C, 37.08; H, 5.12; Fe, 13.70; N, 2.62]. This compound is extremely air-sensitive, especially in solution. Observations suggest that $[Fe_4Te_4(SPh)_4]^{3-}$ is a poorly stable species: prolonged standing or heating of its solutions have led to the separation of black intractable solids together with a variable amount of $[Fe(SPh)_4]^{2-}$ anion. Stability in DMSO solutions was checked by $^1$H NMR which gave no substantial changes over a period of 3 h. Stability appeared much lower in other solvents where it is soluble (DMF, $CH_3CN$, $CH_3NO_2$).

**Collection and Reduction of X-ray Data.** Suitable single crystals of $(Et_4N)_3[Fe_4Te_4(SPh)_4]$ were obtained directly from the above preparation. Crystals were coated with a thin paraffin film to prevent air oxidation. Data collections were carried out at room temperature on a Enraf-Nonius CAD4 automated four-cycle diffractometer equipped with a graphite monochromator. Details of crystal data and refinement are given in Table I. Orientation matrices and unit cell parameters were obtained from 15 machine-centered reflections. Intensities of three check reflections were monitored every 270 reflections. Their intensities showed a 20% decrease over the duration of data collection. Because of this behavior a decay correction was applied to the data on the basis of these standards. An analytical absorption correction was applied to the complete data set. Systematic absences are consistent with the orthorhombic space group *Fdd*2 (no. 43).

**Structure Solution and Refinement.** The structure was solved by the heavy-atom method. The refinement was based on $F_o$, the function minimized being $\sum w(|F_o| - |F_c|)^2$, where $w = 1/\sigma^2(F_o)$. Full-matrix least-squares refinements were carried out by using anisotropic thermal parameters for all the non-hydrogen atoms except for the carbon atoms of the phenyl rings. Phenyl rings were treated as rigid groups. The hydrogen atoms were introduced in calculated positions (C–H = 1.08 Å) but not refined, with an isotropic thermal parameter $U$ = 0.06. At convergence final $R$ and $R_w$ factors defined as $R = \sum||F_o| - |F_c||/\sum|F_o|$ and $R_w = [\sum w(|F_o| - |F_c|)^2/\sum|F_o|^2]^{1/2}$ were 0.0452 and 0.0447, respectively. All the crystallographic calculations were performed on a IBM Personal System 2 computer by using SHELX-76 and ORTEP programs.[8] Atomic scattering factors of the neutral atoms were taken from ref 9. Both the $f'$ and $f''$ of the anomalous dispersion correction were included for the non-hydrogen atoms.[10]

Table II. Valence Ionization Potentials and Coefficients and Exponents of the Slater Atomic Functions[a] Used in the Extended Hückel Calculations

| atom type | orbital | VSIP, eV | $c_1$ | $\zeta_1$ | $c_2$ | $\zeta_2$ |
|---|---|---|---|---|---|---|
| Fe | 3d | −12.70 | 0.5366 | 5.35 | 0.6678 | 1.80 |
| | 4s | −9.17 | 1.0000 | 1.90 | | |
| | 4p | −5.37 | 1.0000 | 1.90 | | |
| S | 3s | −20.00 | 1.0000 | 2.12 | | |
| | 3p | −13.30 | 1.0000 | 1.83 | | |
| H | 1s | −13.60 | 1.0000 | 1.30 | | |

[a] Double-$\zeta$ functions were used for the d iron orbitals.

The positional parameters for the non-hydrogen atoms (Table SI), complete crystallographic data and data collection details (Table SII), derived positional parameters for atoms in rigid groups (Table SIII), calculated positional parameters for hydrogen atoms (Table SIV), thermal parameters for non-hydrogen atoms (Table SV), and a complete listing of the observed and calculated structure factors are given as supplementary material.[11]

**Other Physical Measurements.** All the experiments were performed under strictly anaerobic conditions. The EPR measurements were carried out on finely powdered samples loaded in standard tubes and prepared under nitrogen atmosphere in a drybox. Spectra were recorded at X-band frequencies and 4.2 K on a Varian E-9 spectrometer equipped with an Oxford Instruments continuous flow cryostat. The magnetic susceptibility of the $(Et_4N)_3[Fe_4Te_4(SPh)_4]$ salt was determined, at 1.35 T, on polycrystalline samples (20–30 mg) with a Faraday DSM-5 susceptometer equipped with an optical display and automatized by an Olivetti M-24 computer. A Bruker BE-15 magnet operating at 4.2–300 K and 0.1–1.5 T was used together with a CF-1200 S Oxford Instruments continuous flow cryostat. A diamagnetic correction of −707 cgsu/mol $\times 10^{-6}$ was applied.[12] The $^1$H-NMR spectra were recorded on a Bruker MSL 200 spectrometer operating at 200 MHz and equipped with a variable temperature control unit accurate to ±0.1 °C. Isotropic shifts were calculated from the relation $(\Delta H/H_0)_{iso} = (\Delta H/H_0)_{obsd} - (\Delta H/H_0)_{dia}$, where diamagnetic reference shift was taken as that of PhSH in DMSO-$d_6$ at ambient temperature = 7.15 ppm. UV–vis absorption spectra were recorded on a Lambda-9 Perkin-Elmer spectrophotometer. Solutions ca. $10^{-4}$ M in DMSO were prepared in a drybox under nitrogen atmosphere by using solvent subjected to at least four cycles of vacuum $N_2$.

**Computational Aspects.** Extended Hückel calculations have been performed with the FORTICON program.[13] The calculations were performed on the model complexes $[Fe_2S_2(SH)_4]^{2-}$ with an idealized $D_{2h}$ symmetry. The following bond distances and angles were fixed. Fe–S–Fe = 70.5°, S–Fe–S = 110°, Fe–S(terminal) = 2.29 Å, and the bond distance Fe–S(bridge) was varied as described in the text. The actual values of the VSIP and coefficients and exponents of the Slater functions are collected in Table II.

## Results and Discussion

**Synthesis.** Preparation of tetranuclear iron–chalcogenide trianion clusters $[Fe_4X_4(SR)_4]^{3-}$ has been achieved in previous years through reduction of the preisolated corresponding oxidized dianions $[Fe_4X_4(SR)_4]^{2-}$ by sodium acenaphthylenide[2,14-17] or in the

(8) (a) Sheldrik, G. SHELX-76 *System of Computing Programs*; University of Cambridge: Cambridge, England, 1976. (b) Johnson, C. K. ORTEP; Report ORNL-3794; Oak Ridge National Laboratory: Oak Ridge, TN, 1965.
(9) *International Tables for X-ray Crystallography*; Kynoch: Birmingham, England, 1974; Vol. 4, p 71.
(10) *International Tables for X-ray Crystallography*; Kynoch: Birmingham, England, 1974; Vol. 4, p 148.
(11) See paragraph at the end of paper regarding supplementary material.
(12) Selwood, P. W. *Magnetochemistry*, 2nd ed.; Interscience: New York, 1956.
(13) Hoffmann, R.; Fujimoto, J. R.; Swenson, C.; Wan, C. C. *J. Am. Chem. Soc.* **1973**, *95*, 7644.
(14) Stephan, D. W.; Papaefthymiou, G. C.; Frankel, R. B.; Holm, R. H. *Inorg. Chem.* **1983**, *22*, 1550–1557.
(15) Laskowski, E. J.; Reynolds, J. G.; Frankel, R. B.; Foner, S.; Papaefthymiou, G. C.; Holm, R. H. *J. Am. Chem. Soc.* **1979**, *101*, 6562–6570.
(16) Reynolds, J. G.; Coyle, C. L.; Holm, R. H. *J. Am. Chem. Soc.* **1980**, *102*, 4350–4355.

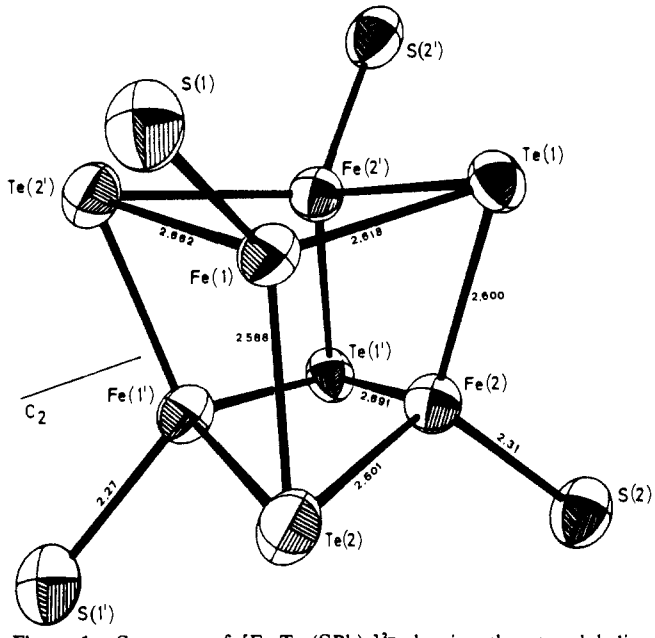


**Figure 1.** Structure of $[Fe_4Te_4(SPh)_4]^{3-}$ showing the atom-labeling scheme, 50% probability ellipsoids, selected interatomic distances (Å), and the location of the crystallographic $C_2$ axis, which relates primed and unprimed atoms. Phenyl rings are omitted for simplicity.

case of R = alkyl through *one-step* synthesis from simple reactants.[18] The extension of this series to the case of X = Te is represented by the present compound, $[Fe_4Te_4(SPh)_4]^{3-}$, for which the spontaneous assembly of four monomeric units $[Fe(SPh)_4]^{2-}$ resulted in the direct formation of the tetrameric one in its reduced form upon addition of a solution of reduced elemental tellurium under anaerobic conditions. Even in this case the species responsible for the partial oxidation of the Fe(II) reactant remains unidentified.[18] Following the procedure used by Gladysz et al. for elemental sulfur and selenium, reduction of tellurium was first realized via reduction with commercially available $LiEt_3BH$ in THF.[19,20] This reaction proceeds rapidly and completely at room temperature and appeared to be very simple and more convenient than the known reduction by $NaBH_4$.[21] The synthesis of an analogous compound, $(Et_3N)[Fe_4Te_4(TePh)_4]$, has been reported by Henkel et al. utilizing a similar procedure, but $NaBH_4$ was used as the tellurium reductant.[22] This was the first report with the larger chalcogenide in the $Fe_4$ unit, though the structure is different from that of the present compound.

**Structure.** The examined compound $(Et_3N)_3[Fe_4Te_4(SPh)_4]$ crystallizes in the *Fdd*2 spatial group, and its structure consists of discrete anions and cations. The cations do not present particular structural characteristics, hence they will not be considered in detail. The anion is constituted by the cluster $[Fe_4Te_4(SPh)_4]^{3-}$ containing the cubane-like unit $[Fe_4Te_4]^+$ analogous to previously described $[Fe_4X_4]^+$ cores.[17,23,24] Its structure is depicted in Figure 1. Selected bond distances and angles are reported in Table III. The crystallographic $C_2$ axis imposed on the anionic cluster passes through the centroids of the two opposite faces of the $[Fe_4Te_4]^+$

**Table III.** Selected Interatomic Distances (Å) and Angles (deg) for $(Et_4N)_3[Fe_4Te_4(SPh)_4]$

| | | | |
|---|---|---|---|
| **Core** | | | |
| Fe(1)-Te(1) | 2.618 (5) | Fe(1)···Fe(1') | 2.793 (6) |
| Fe(1)-Te(2) | 2.588 (4) | Fe(1)···Fe(2) | 2.878 (6) |
| Fe(1)-Te(2') | 2.662 (4) | Fe(1)···Fe(2') | 2.758 (6) |
| Fe(2)-Te(1) | 2.600 (4) | Fe(2)···Fe(2') | 2.844 (5) |
| Fe(2)-Te(2) | 2.601 (6) | | |
| Fe(2)-Te(1') | 2.691 (4) | Te(1)···Te(1') | 4.351 (2) |
| | | Te(1)···Te(2) | 4.104 (3) |
| Fe(1)···Te(1') | 4.349 (4) | Te(1)···Te(2') | 4.448 (3) |
| Fe(2)···Te(2') | 4.361 (5) | Te(2)···Te(2') | 4.337 (2) |
| Fe(1)-Te(1)-Fe(2) | 66.9 (1) | Fe(1')-Fe(1)-Fe(2) | 58.2 (1) |
| Fe(1)-Te(1)-Fe(2') | 62.6 (1) | Fe(1')-Fe(1)-Fe(2') | 62.5 (1) |
| Fe(2')-Te(1)-Fe(2) | 65.0 (1) | Fe(2)-Fe(1)-Fe(2') | 60.6 (1) |
| Fe(1)-Te(2)-Fe(2) | 67.4 (1) | Fe(1)-Fe(2)-Fe(1') | 59.4 (1) |
| Fe(1)-Te(2)-Fe(1') | 64.3 (1) | Fe(1)-Fe(2)-Fe(2') | 57.6 (1) |
| Fe(1')-Te(2)-Fe(2) | 63.2 (1) | Fe(2')-Fe(2)-Fe(1') | 61.8 (1) |
| Te(1)-Fe(1)-Te(2) | 104.1 (2) | Te(2')-Te(1)-Te(1') | 55.6 (1) |
| Te(1)-Fe(1)-Te(2') | 114.8 (2) | Te(2)-Te(1)-Te(1') | 63.4 (1) |
| Te(2)-Fe(1)-Te(2') | 111.4 (1) | Te(2)-Te(1)-Te(2') | 60.8 (1) |
| Te(1)-Fe(2)-Te(2) | 104.2 (1) | Te(1)-Te(2)-Te(2') | 63.5 (1) |
| Te(1)-Fe(2)-Te(1') | 110.6 (1) | Te(1)-Te(2)-Te(1') | 61.0 (1) |
| Te(2)-Fe(2)-Te(1') | 114.4 (1) | Te(2')-Te(2)-Te(1') | 55.7 (1) |
| **Terminal Ligands** | | | |
| Fe(1)-S(1) | 2.27 (1) | S(1)-Fe(1)-Te(1) | 118.3 (2) |
| Fe(2)-S(2) | 2.31 (1) | S(1)-Fe(1)-Te(2) | 117.3 (3) |
| | | S(1)-Fe(1)-Te(2') | 91.1 (2) |
| S(1)-C(1) | 1.77 (2) | S(2)-Fe(2)-Te(1) | 115.5 (3) |
| S(2)-C(7) | 1.77 (2) | S(2)-Fe(2)-Te(2) | 118.3 (2) |
| | | S(2)-Fe(2)-Te(1') | 93.9 (2) |

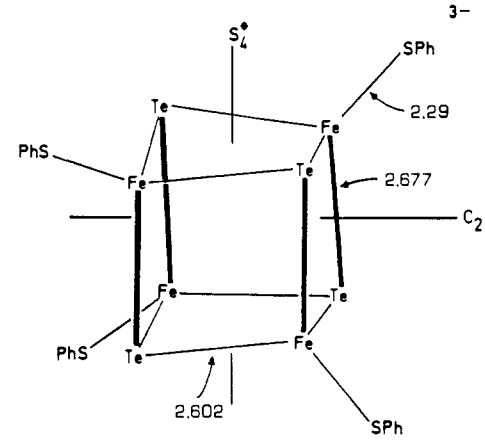


**Figure 2.** Schematic representation of the cubane-like structure of $[Fe_4Te_4(SPh)_4]^{3-}$. Mean values (Å) of short and long (bold line) Fe–Te bonds and Fe–S terminal bonds and crystallographic and idealized (*) symmetry axes are indicated.

core represented by the nonplanar $Fe_2Te_2$ rhomboids. Under crystallographic $C_2$ symmetry only two of the Fe and Te atoms of the cluster are symmetry independent, and thus six Fe–Te bond distances are independent. However, the structure can be represented by an idealized symmetry higher than the crystallographic one. The Fe–Te bond lengths can be partitioned into sets of four "long" (mean value 2.677 Å) and eight "short" (mean value 2.602 Å). Therefore the core presents a tetragonal distortion from cubic symmetry towards an *elongated* $D_{2d}$ symmetry, shown in Figure 2, in which the crystallographic binary axis is approximately perpendicular to the elongation direction defined by an idealized $\bar{4}^*$ axis (the short and long bonds are respectively normal and parallel to this axis). In the *elongated* $D_{2d}$ idealized symmetry, the nonbonded Fe···Fe and Te···Te distances are also divided into two short (perpendicular to the $\bar{4}^*$ axis) and four long (parallel to the $\bar{4}^*$ axis) bonds. However, in this case, these lengths do not rigorously conform to such a symmetry. The distances Fe···Fe are divided into sets of long and short ones but the long ones lie in the faces normal to the $\bar{4}^*$ axis. The distances Te···Te show a spreading of the short ones in a range of 0.11 Å. Such deviations

(17) Laskowski, E. J.; Frankel, R. B.; Gillum, W. O.; Papaefthymiou, G. C.; Renaud, J.; Ibers, J. A.; Holm, R. H. *J. Am. Chem. Soc.* **1978**, *100*, 5322–5337.
(18) Hagen, K. S.; Watson, A. D.; Holm, R. H. *Inorg. Chem.* **1984**, *23*, 2984.
(19) Gladysz, J. A.; Wong, V. K.; Jick, B. S. *J. Chem. Soc., Chem. Commun.* **1978**, 838.
(20) Gladysz, J. A.; Hornby, J. L.; Garbe, J. E. *J. Org. Chem.* **1978**, *43*, 1204.
(21) Di Vaira, M.; Peruzzini, M.; Stoppioni, P. *Angew. Chem., Int. Ed. Engl.* **1987**, *26*, 916.
(22) Simon, W.; Wilk, A.; Krebs, B.; Henkel, G. *Angew. Chem., Int. Ed. Engl.* **1987**, *26*, 1009–1010.
(23) Bobrik, M. A.; Laskowski, E. J.; Johnson, R. W.; Gillum, W. O.; Berg, J. M.; Hodgson, K. O.; Holm, R. H. *Inorg. Chem.* **1978**, *17*, 1402–1410.
(24) Berg, J. M.; Hodgson, K. O.; Holm, R. H. *J. Am. Chem. Soc.* **1979**, *101*, 4586–93.

Table IV. Comparison Among Mean Values of Selected Distances (Å) and Bonding Angles (deg) for $[Fe_4X_4(SPh)_4]^{3-}$ (X = S, Se, or Te) Clusters[a]

| | X | | | |
|---|---|---|---|---|
| | S[b] | S[c] | Se[c] | Te[d] |
| Fe···Fe | 2.74 (2) | 2.73 (2) | 2.78 (4) | 2.82 (5) |
| | [2.750] | [2.728] | [2.777] | [2.798] |
| | [2.730] | [2.720] | [2.782] | [2.878] |
| Fe–X | 2.31 (3) | 2.31 (3) | 2.43 (4) | 2.63 (4) |
| | [2.351] | [2.344] | [2.488] | [2.677] |
| | [2.288] | [2.287] | [2.403] | [2.602] |
| X···X | 3.66 (4) | 3.68 (7) | 3.93 (9) | 4.3 (1) |
| | [3.685] | [3.699] | [3.969] | [4.379] |
| | [3.605] | [3.607] | [3.808] | [4.104] |
| Fe–S | 2.295 (7) | 2.299 (8) | 2.30 (2) | 2.29 (3) |
| X–Fe–X | 104.8 | 104.9 | 106.9 | 109.9 |
| Fe–X–Fe | 72.9 | 72.6 | 69.8 | 64.9 |

[a] The numbers between round brackets indicate the standard deviation of the estimated mean value as $[(\sum x_i^2 - n\bar{x}^2)/(n-1)]^{1/2}$. Those between squared brackets indicate in the following order the mean values of the long and short bonds individualized from the elongated $D_{2d}$ symmetry (see text). [b] $Et_3MeN^+$ salt, ref 16, mean value of two independent anions. [c] $Me_4N^+$ salt, ref 2. [d] $Et_4N^+$ salt, this work.

Table V. Mean Values[a] for the Larger and the Smaller $\theta$ = X–Fe–SR Angles in $[Fe_4X_4(SPh)_4]^{3-}$ and Their Difference $\delta$

| compound | $\theta_{large}$ | $\theta_{small}$ | $\delta$ |
|---|---|---|---|
| $(Me_4N)_3[Fe_4S_4(SPh)_4]\cdot 2MeCN$[b] | 118.2 | 104.3 | 13.9 |
| $(Me_4N)_3[Fe_4Se_4(SPh)_4]\cdot 2MeCN$[b] | 119.2 | 96.6 | 22.6 |
| $(Et_4N)_3[Fe_4Te_4(SPh)_4]$[c] | 117.4 | 92.5 | 24.9 |

[a] In degrees. [b] Reference 2. [c] This work.

from the $D_{2d}$ symmetry are common also to the analogue sulfur and selenium containing compounds $[Fe_4S_4(SPh)_4]^{3-}$ and $[Fe_4Se_4(SPh)_4]^{3-}$, whereas they are much more reduced in $[Fe_4S_4(S\text{-}tBu)_4]^{3-}$ and $[Fe_4S_4(SEt)_4]^{3-}$.[18] In the previously synthesized, tellurium-containing compound $[Fe_4Te_4(TePh)_4]^{3-}$ the core structure was found to be distorted toward an idealized $D_{2d}$ compressed symmetry.[22] In Table IV are reported the more significant mean distances and angles for S, Se, and Te compounds. As expected from the increase of the dimensions of the bridging chalcogenide, an increase of the mean distances Fe···Fe, X···X, and Fe···X in the series S, Se, and Te is evident. The angles to the vertices of the Fe tetrahedron X–Fe–X increase, and those of the calcogen Fe–X–Fe decrease progressively in the series. The elongation entity increases passing from sulfur to selenium and then to tellurium, in terms of the differences between the averages of the long and short Fe–X bonds (0.057 Å, S; 0.085 Å, Se; 0.075 Å, Te) and X···X distances (0.080 Å, S; 0.161 Å, Se; 0.275 Å, Te). Such structures show a greater deviation from the idealized elongated $D_{2d}$ symmetry as the chalcogen atomic number is increased. The deviation is manifested by the progressive distortion of the $Fe_4$ unit. In fact, the average of the long Fe···Fe bonds, i.e., those parallel to the $\bar{4}^*$ axis, assumes values smaller than the average of the short ones in the selenium-containing cluster and much more in the tellurium derivative. The iron sites are distorted in an angular sense from the $C_{3v}$ local symmetry: for every independent iron atom there are two relatively large and one substantially smaller RS–Fe–X angles, and also this effect is progressively much more pronounced in the series S, Se, and Te (Table V).

**Electronic Absorption Spectrum.** The electronic absorption spectrum of $[Fe_4Te_4(SPh)_4]^{3-}$, reported in Figure 3, is dominated by two bands in the region from 300 to 600 nm ($\lambda_{max}$, nm ($\epsilon$, $cm^{-1}$ $M^{-1}$) 303 (45 540), 470 (sh, 5700) in DMSO). In analogy with the tentative assignment made for $Fe_4S_4$ and $Fe_4Se_4$ cluster-containing compounds these bands might be assigned as ligand-to-metal charge-transfer transitions.[3,23,25,26] Previous observations show that the replacement of sulfur with selenium in ferredoxin analogues as well as in otherwise identical complexes has the general effect of decreasing ligand-to-metal charge-transfer energies:[23] this rule seems to be valid also for tellurium substitution.

Table VI. Best-Fitting Parameters for the Magnetic Susceptibility of Some $[Fe_4X_4]^+$ (X = S, Se, Te) Clusters

| compound | $J$ ($cm^{-1}$) | $\alpha = J'/J$ |
|---|---|---|
| $(Et_4N)_3[Fe_4Te_4(SPh)_4]$ | 30.5 (3) | 1.75 (2) |
| $(Me_4N)_3[Fe_4Se_4(SPh)_4]2\cdot MeCN$[a] | 65.3 (3) | 1.69 (1) |
| $(Me_4N)_3[Fe_4S_4(SPh)_4]2\cdot MeCN$[a] | 114.7 (4) | 1.68 (2) |
| $(Et_4N)_3[Fe_4S_4(SPh)_4]$[b] | 109.7 (4) | 1.47 (3) |

[a] Experimental data from ref 2. [b] Experimental data from ref 31.

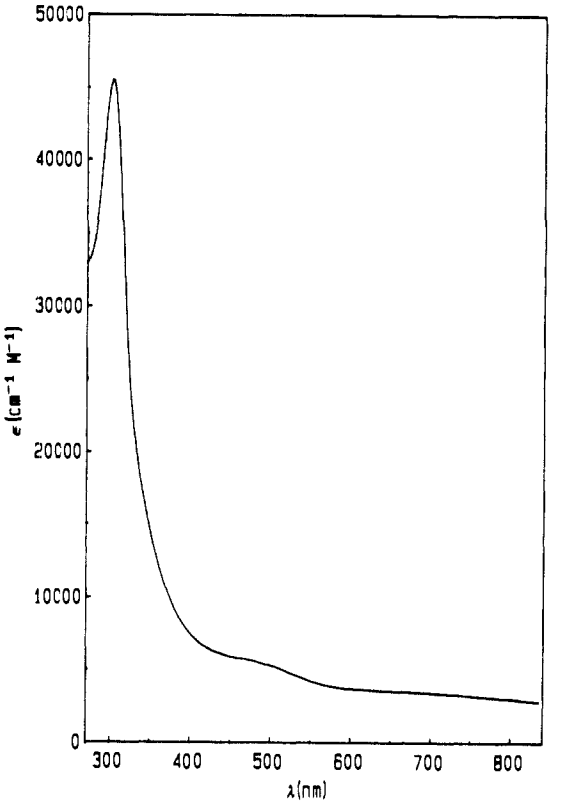


Figure 3. Electronic absorption spectrum of $[Fe_4Te_4(SPh)_4]^{3-}$ in $Me_2SO$ at 298 K.

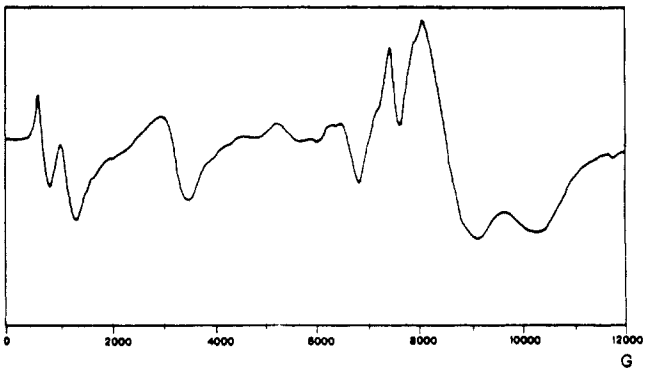


Figure 4. Polycrystalline powder EPR spectra of $(Et_4N)_3[Fe_4Te_4(SPh)_4]$ recorded at X-band at 4.2 K.

**EPR Spectra.** The polycrystalline powder spectrum of $(Et_4N)_3[Fe_4Te_4(SPh)_4]$ recorded at X-band at 4.2 K is shown in Figure 4. The spectrum was found to be sensitive to the sample preparation indicating that some decomposition occurs. Any EPR signal disappears for temperatures above ≈10 K.

In order to try an assignment of the features of the spectra we recorded also single-crystal EPR spectra by rotating one crystal of the title compound around $c$, which in orthorhombic symmetry is one of the principal directions of the **g** tensor. Two intense signals in the range 0.8–1.0 T are observed with angular depen-

(25) Cambray, J.; Lane, R. W.; Wedd, A. G.; Johnson, R. W.; Holm, R. H. *Inorg. Chem.* **1977**, *16*, 2565–2571.
(26) Aizman, A.; Case, D. A. *J. Am. Chem. Soc.* **1982**, *104*, 3269–3279.

dence typical of a Kramers doublet, which were attributed to the two magnetically nonequivalent centers present in the unit cell. The line widths and intensities of the signals of the Kramers doublet was found to be dependent on the orientation. The signals, in fact, broadened and became unobservable in the crystallographic available orientations perpendicular to $c$.

The spectra measured in the $c$ rotation can be interpreted with an effective $S' = 1/2$ spin Hamiltonian with $g$ values $g_x = 0.812$ and $g_y = 0.646$. These $g$ values correspond nicely to two of the most intense features seen in the polycrystalline spectrum.

Although a detailed analysis of the EPR spectra is not possible on these grounds, the measured $g$ values are typical of a Kramers doublet originating from a quartet state largely split by zero-field splitting.[27]

**Magnetic Behavior.** The temperature dependence of the magnetic susceptibility of $(Et_4N)_3[Fe_4Te_4(SPh)_4]$ measured on a polycrystalline sample is reported in Figure 5a. Also these measures were found to depend on the sample preparation, unless they are performed on a freshly prepared sample kept under nitrogen atmosphere. In Figure 5a the circles represent the experimental points, and the lines are computed by using the procedure described below.

In order to interpret the magnetic measurements we use the Heisenberg–Dirac–Van Vleck spin Hamiltonian to parameterize the exchange interaction between the iron centers. A formal attribution of the oxidation states to the individual iron centers shows that the cluster is formed by three iron(II) and one iron(III) centers. This picture is not consistent, anyway, with the molecular structure which shows only two crystallographically inequivalent iron atoms, and a better picture should include electron delocalization of the magnetic electrons over the spin centers. This view has already been adopted to interpret the low-temperature magnetic behavior of $Fe_3S_4$ clusters.[6] The effect of the delocalization of the magnetic electrons provides a coupling mechanism, often referred to as *double exchange*, which in principle is different from the isotropic Heisenberg–Dirac–Van Vleck spin coupling. In dinuclear systems this effect was already studied by Zener[28] and Anderson and Hasegawa[29] and more recently by Girerd et al.,[5] and it was found to produce a resonance splitting of the total spin multiplets arising from the isotropic exchange stabilizing the highest spin state, thus giving a ferromagnetic contribution to the exchange interaction. For trinuclear mixed-valence systems Belinskii[30] found a similar splitting, but the actual spin-level ordering was found to depend more critically on the $p/J$ ratio, where $p$ is the transfer integral and $J$ is the exchange parameter: in particular the presence of double exchange does not always induce an overall ferromagnetic interaction. In low-symmetry systems the presence of double exchange cannot be uniquely determined from magnetic measurements alone, and a number of mixed-valence clusters have been analyzed by using the simpler Heisenberg–Dirac–Van Vleck spin Hamiltonian. The mixed valence character of some iron clusters was recognized through magnetic Mössbauer measurements[6] which gave a number of information complementary to the magnetic susceptibility.

In the following we will neglect the possibility of valence delocalization, and we will describe the exchange interaction through the simplest spin Hamiltonian

$$\mathcal{H} = J(\mathbf{S}_1\cdot\mathbf{S}_2 + \mathbf{S}_1\cdot\mathbf{S}_3 + \mathbf{S}_2\cdot\mathbf{S}_3) + J'(\mathbf{S}_1\cdot\mathbf{S}_4 + \mathbf{S}_2\cdot\mathbf{S}_4 + \mathbf{S}_3\cdot\mathbf{S}_4) \quad (1)$$

where $S_1 = S_2 = S_3 = 2$ represent the iron(II) centers and $S_4 = 5/2$ is the iron(III) one, and $J$ and $J'$ are the iron(II)–iron(II) and iron(II)–iron(III) isotropic exchange coupling constants, respectively. The Hamiltonian (1) is the most simple spin-coupling model to describe the exchange interaction in $(Et_4N)_3[Fe_4Te_4(SPh)_4]$, behind the symmetric one with $J = J'$, and the symmetry of the real system can be lower than that described in (1). Furthermore it must also be remembered that anisotropic terms of the type $\mathbf{S}\cdot\mathbf{D}\cdot\mathbf{S}$, where $\mathbf{D}$ is a symmetric traceless second rank tensor, can have importance in (1) especially when they represent the single ion iron(II) zero-field splitting. Inclusion of these terms in (1) as well as allowing for low symmetries will increase the number of the parameters required for fitting the magnetic data, and we will rest on the most simple Hamiltonian (1) as long as it will work. It is important to note that due to all the approximations made, which are common to other authors as well,[31] the $J$ and $J'$ values should be seen as an estimate of the exchange interaction useful to make comparisons between series of compounds.

The eigenvalue of (1) can be conveniently computed on a spin basis obtained through the vector coupling scheme $S_{12} = S_1 + S_2$, $S_{123} = S_{12} + S_3$, and $S = S_{123} + S_4$. Hamiltonian (1), in fact, commutes with $S_{12}^2$, $S_{123}^2$, $S^2$, and $S_z$, and it is therefore diagonal in the $\{S_{12}S_{123}S\}$ basis, each state being $2S+1$-fold degenerate. The energies of the states are given by

$$E(S_{12}S_{123}S) = J/2[S_{123}(S_{123} + 1) - 18] + J'/2[S(S + 1) - S_{123}(S_{123} + 1) - 35/4] \quad (2)$$

It should be noted that (2) is independent from $S_{12}$, and the energies are thus grouped in degenerate manifolds having the same value of $S$ and $S_{123}$ and different $S_{12}$ values. This symmetry was not found in a previous work.[31]

The temperature dependence of the magnetic susceptibility can be computed by using (2) and the reported expression.[32] In Figure 5a the dotted curves have been computed by using $g = 2.00$ and $J = 30.54$ cm$^{-1}$. The solid line has been obtained through a fitting procedure by minimizing the function

$$F = \sum_i [(\chi_i^{obsd} - \chi_i^{calcd})^2/(\chi_i^{obsd})^2] \quad (3)$$

using a Simplex routine with $J$ and $\alpha = J'/J$ as free parameters. With this procedure we have fitted also the magnetic data reported for $(Et_4N)_3[Fe_4S_4(SPh)_4]$ and $(Me_4N)_3[Fe_4X_4(SPh)_4]\cdot 2MeCN$ (X = S, Se). The results of the fitting are graphically shown in Figure 5b–d and are reported in Table VI. In $(Me_4N)_3[Fe_4S_4(SPh)_4]\cdot 2MeCN$, $(Me_4N)_3[Fe_4Se_4(SPh)_4]\cdot 2MeCN$, and $(Et_4N)_3[Fe_4Te_4(SPh)_4]$ the ground state corresponds to $S = 3/2$ and three states are degenerate, namely $|4\ 4\ 3/2\rangle$, $|3\ 4\ 3/2\rangle$, and $|2\ 4\ 3/2\rangle$. For $(Et_4N)_3[Fe_4S_4(SPh)_4]$ the ground state is $S = 1/2$ and the four states $|4\ 3\ 1/2\rangle$, $|3\ 3\ 1/2\rangle$, $|2\ 3\ 1/2\rangle$, and $|1\ 3\ 1/2\rangle$ are degenerate. It must be noted that the computed curves do not reproduce the experimental data for temperatures below $\approx$10 K when the ground state is $S = 3/2$. This is most probably due to the zero-field splitting of the ground state which we have neglected in our model. As a matter of fact, zero-field splitting as large as 6 cm$^{-1}$ has been measured in some $Fe_4S_4$ cluster.[33] The EPR spectra confirm the nature of the ground state and that zero-field splitting is large enough to leave an isolated Kramers doublet as the ground state at liquid helium temperature. It is quite meaningful that the simplest theoretical approach is capable of accounting for the essential features of the temperature dependence of the magnetic data. Thus double exchange cannot be uniquely determined by magnetic measurements alone, although its inclusion can alter the absolute value of the exchange parameters.[34] The computed $\alpha$ values are 1.68 (2), 1.69 (1), and 1.75

(27) Bencini, A.; Gatteschi, D. *Transition Metal Chemistry*; Melson, G. A., Figgis, B. N., Eds.; **1982**, *8*, 1.
(28) Zener, C. *Phys. Rev.* **1951**, *82*, 403.
(29) Anderson, P. W.; Hasegawa, H. *Phys. Rev.* **1955**, *100*, 675.
(30) Belinskii, M. I. *Mol. Phys.* **1987**, *60*, 793.
(31) Papaefthymiou, G. C.; Laskowski, E. J.; Frota-Pessoa, S.; Frankel, R. B.; Holm, R. H. *Inorg. Chem.* **1982**, *21*, 1723–1728.
(32) Griffith, J. S. *Structure and Bonding* **1972**, *10*, 87.
(33) Carney, M. J.; Papaefthymiou, G. C.; Frankel, R. B.; Holm, R. H. *Inorg. Chem.* **1989**, *28*, 1497–1503.
(34) Other models have been used to fit the data.[7] With three $J$ values (one for the couple Fe(II)–Fe(III), one for each member of the couple and Fe(II), the third among Fe(II) ions) the fitting is quite satisfactory though the correlation coefficients among the $J$ values are 85–98%, and the ground state may be not correctly predicted. If the resonance delocalization parameter $B$ is also included, either with two $J$ or three $J$ parameters, satisfactory fittings are obtained, but the correlation coefficients among the parameters are always larger than 80%. Only when other data on the nature of the ground state is available should a more sophisticated model (with more than two parameters) including electronic delocalization be developed. Furthermore small variations of $g$ lead to small variations of $J$; in any case it does not affect the conclusions reached here.

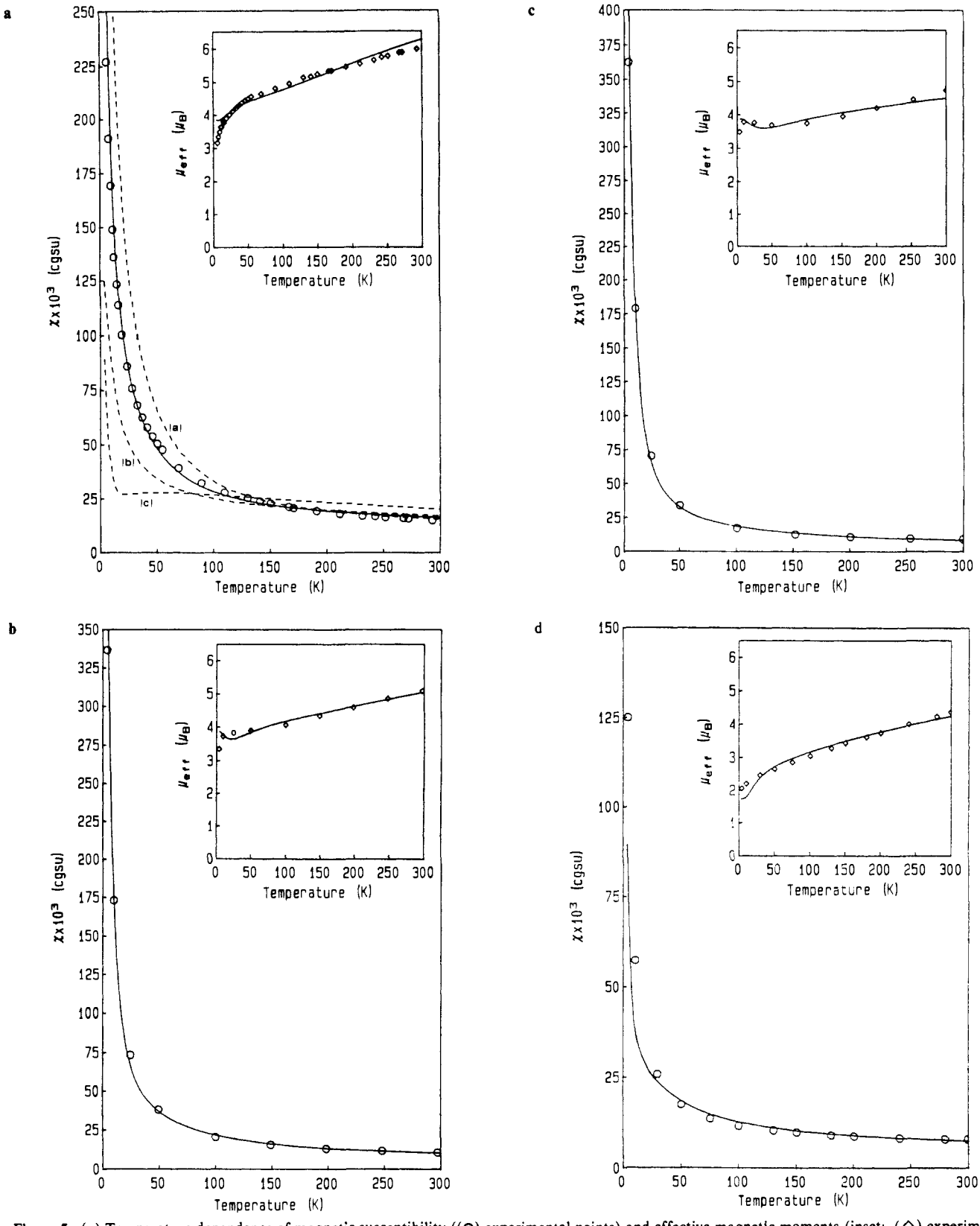


**Figure 5.** (a) Temperature dependence of magnetic susceptibility ((○) experimental points) and effective magnetic moments (inset: (◇) experimental points) for $(Et_4N)_3[Fe_4Te_4(SPh)_4]$. The dotted lines are computed with the following values: $g = 2.00$, $J = 30.5$ cm$^{-1}$, and (a) $\alpha = 2$, (b) $\alpha = 1.5$, and (c) $\alpha = 1$. The solid lines are the theoretical simulations corresponding to the best fit parameters for the $\chi$ experimental data: $J = 30.5$ cm$^{-1}$ and $\alpha = 1.75$. (b) Magnetic data for $(Me_4N)_3[Fe_4Se_4(SPh)_4]\cdot 2MeCN$. Explanations are the same in Figure 5a. Experimental data are from ref 2. Best fit parameters for the $\chi$ data: $J = 65.3$ cm$^{-1}$, $\alpha = 1.69$. (c) Magnetic data for $(Me_4N)_3[Fe_4S_4(SPh)_4]\cdot 2MeCN$. Explanations as the same as in Figure 5a. Experimental data are from ref 2. Best fit parameters for the $\chi$ data: $J = 114.7$ cm$^{-1}$, $\alpha = 1.68$. (d) Magnetic data for $(Et_4N)_3[Fe_4S_4(SPh)_4]$. Explanations are the same as in Figure 5a. Experimental data are from ref 31. Best fit parameters for the $\chi$ data: $J = 109.7$ cm$^{-1}$, $\alpha = 1.47$.

(2) for $(Me_4N)_3[Fe_4S_4(SPh)_4]\cdot 2MeCN$. $(Me_4N)_3[Fe_4S_4(SPh)_4]\cdot 2MeCN$, and $(Et_4N)_3[Fe_4Te_4(SPh)_4]$, respectively, and 1.47 (3) for $(Et_4N)_3[Fe_4S_4(SPh)_4]$. The nature of the ground state therefore seems to be determined by the $\alpha$ value, i.e., the ratio between the Fe(III)–Fe(II) and the Fe(II)–Fe(II) exchange coupling constants, while the exchange interactions remain an-

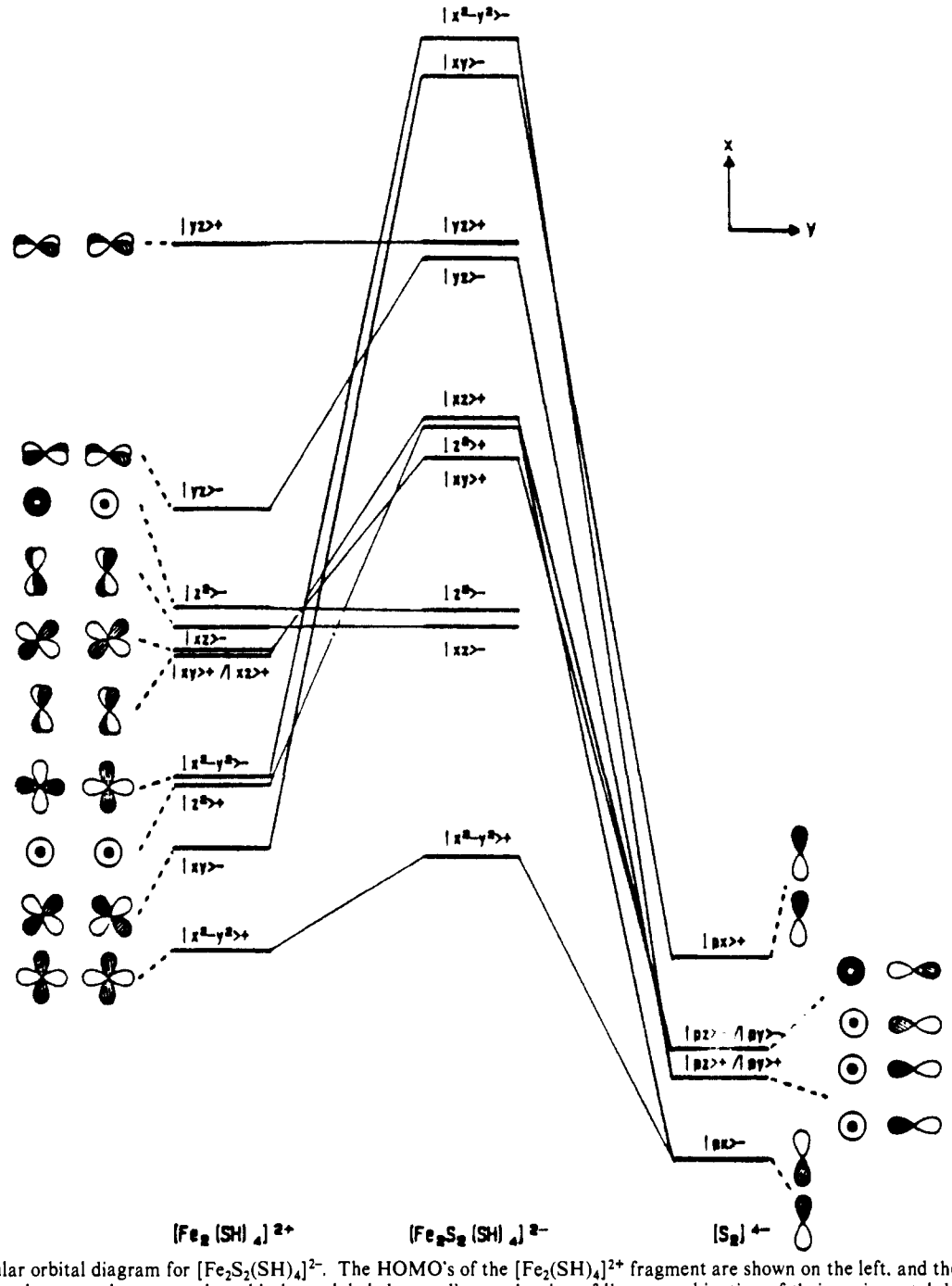


Figure 6. Molecular orbital diagram for $[Fe_2S_2(SH)_4]^{2-}$. The HOMO's of the $[Fe_2(SH)_4]^{2+}$ fragment are shown on the left, and the HOMO's of the whole complex are shown on the center; the orbitals are labeled according to the sign of linear combination of their main metal d component. The relevant molecular orbital for the $S_2^{4-}$ fragment are shown on the right labeled accordingly to the main component of sulfur atomic orbitals.

tiferromagnetic in all the series. The strength of the interaction decreases on passing from S to Te from $J = 114.7$ (4) $cm^{-1}$ to $J = 30.5$ (3) $cm^{-1}$. The values of $\simeq 115$ $cm^{-1}$ for Fe(II)-Fe(II) and $\simeq 190$ $cm^{-1}$ for Fe(III)-Fe(II) are consistent with the values found for similar systems.[35,36]

**The Orbital Model of the Exchange Interaction.** From the above data we can conclude that the nature of the bridging chalcogen ligand seems to influence the magnitude of the exchange interaction between the iron centers. Quantitative calculations of the exchange interaction in iron sulfur clusters have recently been performed by Noodleman et al. by using the X$\alpha$ theory.[37] These calculations have also shown the delocalized nature of the electrons in these systems. X$\alpha$ calculations have already been found to give useful information on the nature of the exchange interactions in several systems and allowed the quantitative estimate of the $J$ values.[38] Other models are available however that can be used in order to relate the variation of the $J$ values in a series of complexes which are based on more simple extended Hückel calculations.[38,39]

In order to look at the effect of geometrical variations in the bonding mode of the bridging chalcogens on the pairwise magnetic interaction between the iron centers we applied the orbital model of the exchange interaction[39] to a hypothetical dinuclear unit $[Fe_2S_2(SH)_4]^{2-}$. In this model the exchange interaction between two paramagnetic centers is given as the sum of two contributions

$$J = J_F + J_{AF} \quad (4)$$

(35) Banci, L.; Bertini, I.; Luchinat, C. *Structure and Bonding* **1990**, *72*, 113-135.
(36) Dunham, W. R.; Palmer, G.; Sands, R. H.; Bearden, A. J. *Biochim. Biophys. Acta* **1971**, *253*, 373-384.
(37) Noodleman, L.; Case, D. A.; Sontum, S. F. *J. Chim. Phys.* **1989**, *86*, 743.
(38) Bencini, A. *J. Chim. Phys.* **1989**, *86*, 763.
(39) Hay, P. J.; Thibeault, J. C.; Hoffman, R. *J. Am. Chem. Soc.* **1975**, *97*, 4884.

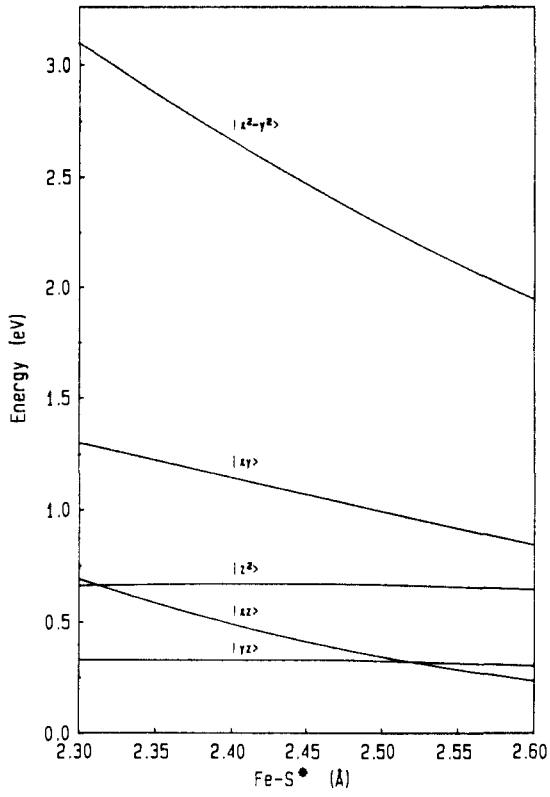


Figure 7. Effect of varying the Fe–S* (bridge) bond length on the energy difference of the highest occupied molecular orbitals of $[Fe_2S_2(SH)_4]^{2-}$.

where $J_F$ represents a ferromagnetic contribution and $J_{AF}$ is an antiferromagnetic one. The antiferromagnetic term is proportional to the square of the energy difference between the molecular orbitals which originate from the homologous magnetic orbitals of the single paramagnetic centers. These energy differences can be easily computed with EHMO theory as a function of geometrical and bonding parameters. Assuming thus that the ferromagnetic term in (4), which contains two electron exchange integrals, does not vary appreciably in the series, useful correlations have been done.[38,39]

In the series of $Fe_4X_4$ clusters which we have studied, the bridging Fe–X–Fe, $\beta$, angle varies together with the nature of X, being $\approx 73°$ for X = S and $\approx 65°$ for X = Te. At the same time the Fe–X and Fe–Fe bond distances increase going from 2.3 and 2.7 to 2.6 and 2.8 Å for X = S and Te, respectively. Since EHMO is a parametric model, we did not try to vary the VSIP and the basis functions of the bridging atom in order to mimic the chemical nature of S, Se, and Te, but we kept them fixed and looked at the effect of geometrical distortions. This procedure surely neglects some important factors, e.g., the nature of the bridging atom, but allows us to focalize our attention on geometrical variations which are also responsible for the magnetic behavior. The Fe–X–Fe angle, $\beta$, does not vary much along the series, and the effect of varying the bridging angle on the energies of the d orbitals in $M_2X_2$ dimers has already been investigated in details.[39] The orbitals most largely affected by this geometrical variation are the linear combinations of the two $d_{x^2-y^2}$ atomic orbitals, and it was found that for $\beta$ larger or smaller than 90° an antiferromagnetic interaction dominates. Thus we kept the $\beta$ angle fixed, and the Fe–S(bridge) distance was varied together with the Fe–Fe one. The other parameters were fixed at the values described in the computational aspects. The results of the calculations for $\beta$ = 73.82°, Fe–S(terminal) = 2.29 Å, and Fe–Fe = 2.75 Å, are shown in Figure 6. Only the highest occupied molecular orbitals, which are the ones relevant to the exchange interactions, are shown. The nature of the molecular orbitals has been analyzed on a fragment basis, the first fragment being $[Fe_2(SH)_4]^{2+}$ and the second $S_2^{4-}$, and the fragment orbitals which symmetry allows to interact are pictorially indicated on the extreme sides of Figure 6. In the pictorial view of the magnetic orbitals of the $[Fe_2(SH)_4]^{2+}$ fragment we have shown only the largest component of the metal orbitals for the sake of simplicity in order to label the orbitals themselves. It can be seen that the $|x^2-y^2\rangle$ and $|xy\rangle$ orbitals undergo the maximum splitting from the interaction with the $|p_x\rangle$ and $|p_y\rangle$ orbitals of sulfur as a result of a more efficient overlap of the in-plane orbitals as compared to the out-of-plane ones. In Figure 7 the computed variation of the energy differences between the two couples of molecular orbitals as a function of the Fe–S distance is shown. It can be seen that the splitting of the $|x^2-y^2\rangle$,

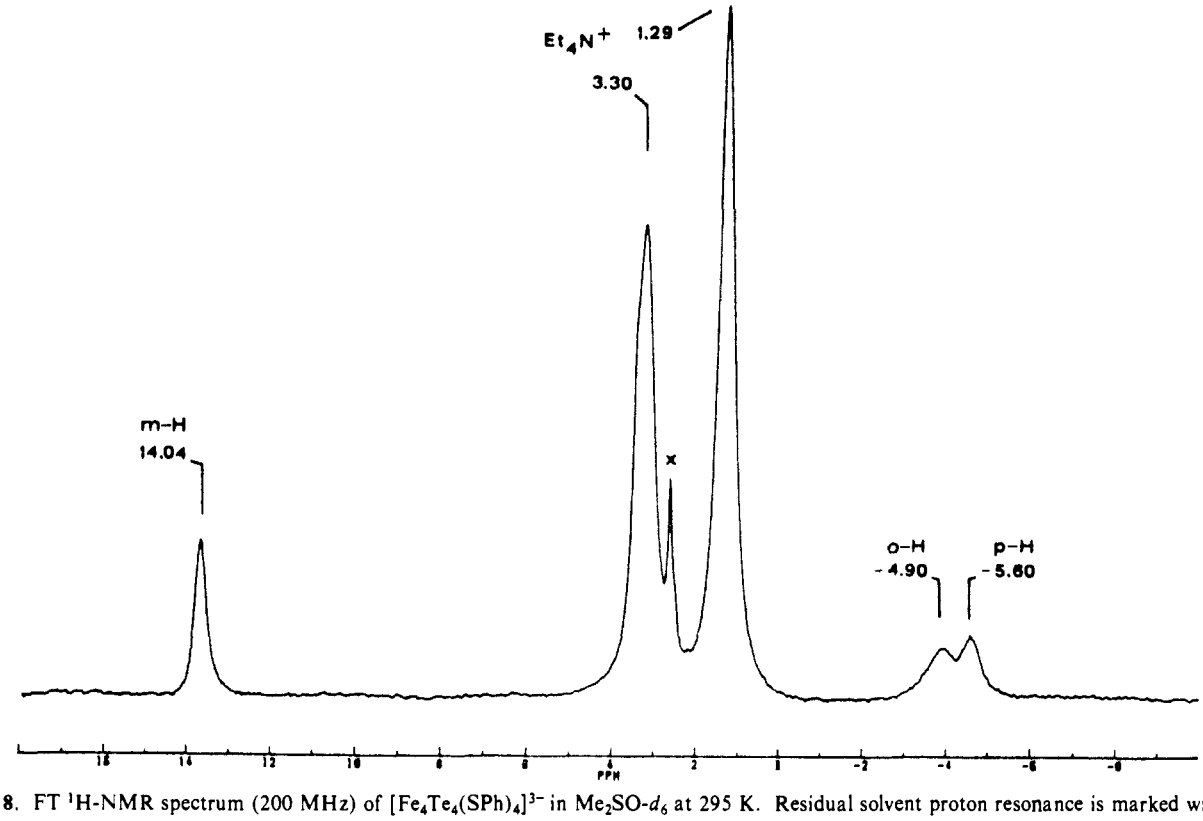


Figure 8. FT $^1$H-NMR spectrum (200 MHz) of $[Fe_4Te_4(SPh)_4]^{3-}$ in $Me_2SO$-$d_6$ at 295 K. Residual solvent proton resonance is marked with an ×.

Table VII. Magnetic Data and $^1$H Chemical Shifts[a] at 298 K for the Synthetic $[Fe_4X_4(SPh)_4]^{3-}$ Clusters (X = S, Se, or Te)

| | | observed shifts (ppm) | | | |
|---|---|---|---|---|---|
| | $\mu$,[b] $\mu_B$ | *o*-H | *m*-H | *p*-H | ref |
| $[Fe_4S_4(SPh)_4]^{3-}$ | 4.72 | 2.17 | 10.4 | 1.63 | 2 |
| $[Fe_4Se_4(SPh)_4]^{3-}$ | 5.10 | −0.61 | 11.6 | −0.61 | 2 |
| $[Fe_4Te_4(SPh)_4]^{3-}$ | 5.99 | −4.56 | 13.98 | −5.24 | this work |

[a] In $Me_2SO$-$d_6$. [b] $\mu = 2.828(\chi T)^{1/2}$.

$|xy\rangle$, and $|xz\rangle$ type orbitals is influenced most by the increase in the bond length, all the other splittings being almost uninfluenced. Since the splitting decreases on increasing the Fe–S distance, a smaller antiferromagnetic interaction is expected as a consequence of this geometrical variation, and this can explain the observed decrease of the $J$ values.

**Nuclear Magnetic Resonance Spectra.** The $^1$H NMR spectrum of $(Et_3N)_3[Fe_4Te_4(SPh)_4]$ in DMSO-$d_6$ at 22 °C is shown in Figure 8. It displays a single set of resonances generated by the phenyl ring protons: the structural and electronic equivalence of the ligands are probably due to fast chemical exchange in solution on the NMR time scale. Previous analyses of the $^1$H NMR spectra of $[Fe_4X_4(SPh)_4]^{3-,2-}$ (X = S or Se) have demonstrated that the isotropic shifts of these clusters are essentially contact in origin and are affected primarily by the RS → Fe (core) antiparallel spin transfer manifested by the alternating sings of *o*-, *m*-, and *p*-H shifts and resulting in parallel spin in sulfur 3p type orbitals allowing spin delocalization on the phenyl ring.[16,40-42] This mechanism affords positive spin density at *o*-C and *p*-C and negative density at *m*-C consistent with results from SCF-X$\alpha$-SW calculations.[43] Consequently, the downfield isotropic shift of *m*-H is indicative of dominant contact shifts. In Table VII are reported the proton chemical shifts and the magnetic moments for the synthetic clusters $[Fe_4X_4(SPh)_4]^{3-}$ (X = S, Se, Te). The larger shifts of the tellurium compared to the sulfur and selenium analogues are consistent with the larger magnetic moments of the former due to smaller antiferromagnetic coupling constants among the irons in the $[Fe_4Te_4]^+$ core. Shifts and magnetic susceptibilities parallel each other providing evidence that also in the tellurium analogue the isotropic shifts are dominantly contact in origin.

The temperature dependence of the isotropically shifted resonances was measured from 22 to 75 °C. The shifts follow the same pattern of the analogous sulfur- or selenium-containing compounds.

## Concluding Remarks

The $Fd_{ox}/Fd_{red}$ electron transfer couple is one of the most pervasive in biology; therefore, it is essential to understand the electronic properties of such system. The synthetic $[Fe_4S_4]^+$ cores are analogues of native-reduced Fd and possess spin state and structural variability possibly as extensive as the biological clusters. Holm and collaborators have demonstrated that polycrystalline synthetic clusters can exist in a variety of ground states.[4] A correlation between the structure and the electronic state of the $[Fe_4X_4]^+$ clusters does not yet exist; the sensitivity of the spin ground states to the extrinsic factors regulating the detailed cluster structure in the solid state is unpredictable. In this study the synthesis and characterization of the $[Fe_4Te_4(SPh)_4]^{3-}$ cluster are described. The experimental data reported and in particular the susceptibility data as well as the previously obtained magnetic data for S and Se analogues can be interpreted with an isotropic Heisenberg spin Hamiltonian.

The theoretical approach allowed us to correlate the ground states, either 1/2 or 3/2 in the various cases, to the $J'/J$ ratio. The $J$ value between $Fe^{2+}$ and $Fe^{3+}$ in $Fe_4S_4^+$ is the same as for the $Fe_2S_2$ proteins.[35,36] We have also discussed the large correlation coefficients between $J$ and the resonance delocalization parameter B. It seems, therefore, that slight changes in the $J$ values, their ratios, and/or the electron delocalization determine the ground state. In an attempt to better understand the factors determining the $J$ values, the relative contributions to them as a function of geometrical parameters have been analyzed in terms of the EHMO theory. The decrease of the $J$ values in passing from sulfur to selenium and to tellurium derivatives can be related, besides other effects, also to a decrease of the antiferromagnetic exchange contribution due to the increase in Fe–chalcogen and Fe–Fe distances.

**Acknowledgment.** We are pleased to acknowledge and thank Franco Cecconi for the skilled technical assistance and Andrea Caneschi for the magnetic susceptibility measurements.

**Supplementary Material Available:** Table SI (positional parameters for the non-hydrogen atom), Table SII (complete crystallographic data and data collection details), Table SIII (derived positional parameters for atoms in rigid groups), Table SIV (calculated positional parameters for hydrogen atoms), and Table SV (thermal parameters for non-hydrogen atoms) (5 pages); Table SVI (observed and calculated structure factors) (6 pages). Ordering information is given on any current masthead page.

(40) Reynolds, J. G.; Holm, R. H. *Inorg. Chem.* **1981**, *20*, 1873–1878.
(41) Reynolds, J. G.; Laskowski, E. J.; Holm, R. H. *J. Am. Chem. Soc.* **1978**, *100*, 5315–5322.
(42) Holm, R. H.; Phillips, W. D.; Averill, B. A.; Mayerle, J. J.; Herskovitz, T. *J. Am. Chem. Soc.* **1974**, *96*, 2109–2117.
(43) Yang, C. Y.; Johnson, K. H.; Holm, R. H.; Norman, J. G. Jr. *J. Am. Chem. Soc.* **1975**, *97*, 6596.